

MONTE CARLO SIMULATION FRAMEWORK FOR TMT

Konstantinos Vogiatzis and George Z. Angeli
TMT Observatory Corp., Pasadena, CA, USA

ABSTRACT

This presentation describes a strategy for assessing the performance of the Thirty Meter Telescope (TMT). A Monte Carlo Simulation Framework has been developed to combine optical modeling with Computational Fluid Dynamics simulations (CFD), Finite Element Analysis (FEA) and controls to model the overall performance of TMT.

The framework consists of a two year record of observed environmental parameters such as atmospheric seeing, site wind speed and direction, ambient temperature and local sunset and sunrise times, along with telescope azimuth and elevation with a given sampling rate. The modeled optical, dynamic and thermal seeing aberrations are available in a matrix form for distinct values within the range of influencing parameters. These parameters are either part of the framework parameter set or can be derived from them at each time-step. As time advances, the aberrations are interpolated and combined based on the current value of their parameters. Different scenarios can be generated based on operating parameters such as venting strategy, optical calibration frequency and heat source control.

Performance probability distributions are obtained and provide design guidance. The sensitivity of the system to design, operating and environmental parameters can be assessed in order to maximize the % of time the system meets the performance specifications.

Keywords: Extremely Large Telescopes, Performance Modeling, Statistical Modeling

1. INTRODUCTION

The objective of observatory system performance modeling is to evaluate the optical effects of various imperfections and disturbances. Most of them are either true random processes (local actuator and sensor noise drift, material and fabrication errors) or depend on environmental and operational parameters. Most operational and obviously all the environmental parameters are stochastic in nature. This latter error category includes mirror support print-through (zenith angle dependence), in-plane segment motion (zenith angle and temperature), thermal deformations of optical surfaces and structure (ambient temperature and heat sources), Alignment and Phasing System (APS) measurements (ambient temperature), wind buffeting (zenith and azimuth angles, ambient wind speed) and mirror and dome seeing (zenith and azimuth angles, ambient wind speed and temperature). The following section describes a strategy that can validate specific subsystem and overall system requirements by investigating the statistical properties of a stochastic variable such as telescope performance.

2. METHODOLOGY

2.1 Motivation - objectives

The performance models developed by the System Engineering group accept as input design, operational and environmental parameters. Besides the random behavior of the inputs, the system's response depends also on its previous state, due primarily to temperature time-scales. Hence, in order to adequately represent these inputs a sufficiently long record of air velocity, turbulence and temperature on the structure surfaces and optical path volume should be compiled, at a sufficiently high sampling rate. These values depend on the external wind speed and direction, the ambient temperature, the orientation of the telescope, the venting efficiency of the enclosure, the existing heat sources and the available observing time. To complete the performance estimate the atmospheric seeing should also be known at the same time instances. Then the models should in principle be able to predict the instantaneous performance of the observatory and obtain a statistically sufficient performance estimate sample. The performance metric used by all models for seeing limited observations is the normalized Point Source Sensitivity (PSSn) [1].

Temperature variations inside the optical path volume (including the optical surfaces), which cause refractive index variations and optical deformation, depend on the ambient temperature variations as the air flows through the vents and across the aperture, the temperature variations of the enclosure and telescope surfaces and the heat sources. Ideally one would track these temperatures and ray-trace through the volume to obtain the resulting aberration at each time-step.

Due to the magnitude of the computational effort involved and the dramatic difference expected between air and solid thermal time scales such a time-domain simulation is not possible for the required period of time. The same holds true to a lesser extent for dynamic disturbances caused by wind. Moreover some of the modeled aberrations are not independent (for instance thermal seeing and wind buffeting) and cannot be investigated separately. It is evident that a framework should be established with acceptable approximations and assumptions to combine the performance estimates and track the overall performance of the observatory.

2.2 Framework

The essence of the performance framework is depicted in Figure 1. Yellow color denotes the available inputs. Cyan shows what can be controlled by design and operation. Green shows the developed models with pre-calculated aberrations in multidimensional matrix form, spanning the range of all influencing parameters (dimensions). Purple corresponds to mathematical/statistical processing and is in fact the core of the time domain simulation. For the reasons described above at least the temperature of the primary mirror should also be tracked throughout the record.

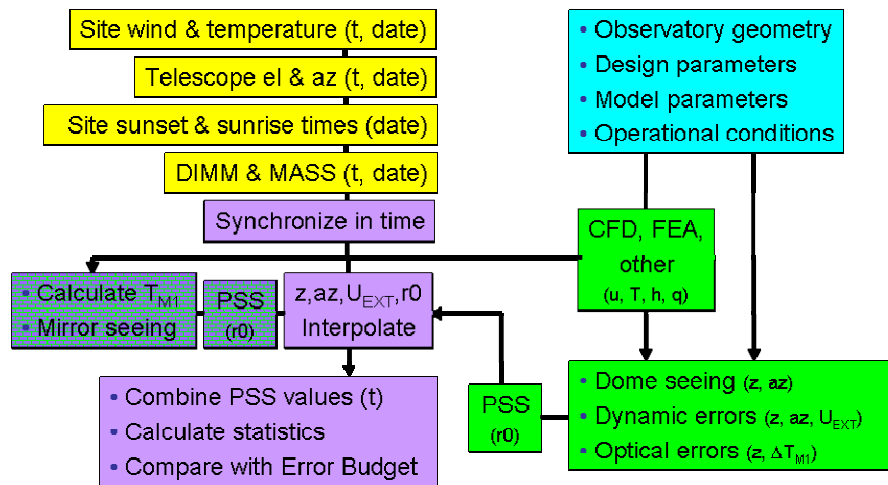


Figure 1. Monte Carlo performance Framework flow chart

3. INPUTS

3.1 Environment

Records of wind speed, direction, temperature.

Site The baseline site is Armazones, Chile. The data are from 2006 and 2007. (Records from CFHT, Mauna Kea, Hawaii and VLT, Paranal, Chile, were also obtained from 2005 and 2006 respectively.)

Period The period of two years was chosen in order to incorporate seasonal variations. The site sunset and sunrise UT times corresponding to the data records have been obtained.

Sampling rate The standard sampling rate is 2min. It is dictated by the availability of weather station and telescope orientation data. It also has to meet the stability criterion of the solid thermal code that solves for temperature through M1. It is also equivalent to at least a flow-through time for the enclosure at 10%-ile external wind speeds, enough for the flow inside the enclosure to establish a large scale pattern. During that time the telescope-enclosure orientation can be considered fixed (0.5° change for tracking).

Height from ground The values should correspond to a height of 20m, which is the average vent height. Unfortunately only the weather station deployed on the site at 2m from ground has provided with records of two years. Therefore appropriate scaling is required to relate the 2m values to the 20m level. Figures A1a and A1b show the scaling factors applied to the night time wind speed and temperature. The factors are compatible with the existing measurements of the Armazones 30m tower [2]. The factors can be applied to the mean velocity and temperature fields. It is expected that at the 20m level the integral scale of turbulence be different by that of 2m. So, at first, one could think that applying the factors to a 2min sampled record is not appropriate. However, only the mean values are sensed by M1, since turbulence is filtered by the vents, when open, and new turbulence is generated by the vent edges. The turbulence levels on M1 are

known through CFD for all wind-telescope relative azimuth angles. In [2] and also Figure A2 it is also shown that the wind speed at 50m is similar to that of 20m, so the same wind speed statistics can be used for M2 forces.

3.2 Atmosphere

Records of DIMM and MASS r_0 from Armazones have also been obtained for the same period of time. The correct r_0 value required for the simulations should exclude the first 60m (the enclosure influence). Since TMT DIMM data are valid above 7m and MASS data above 500m, a combination of both is required. Based on [2], a good approximation is $(r_{0M}+r_{0D})/2$. The resulting cumulative probability distribution is shown in Figure 2.

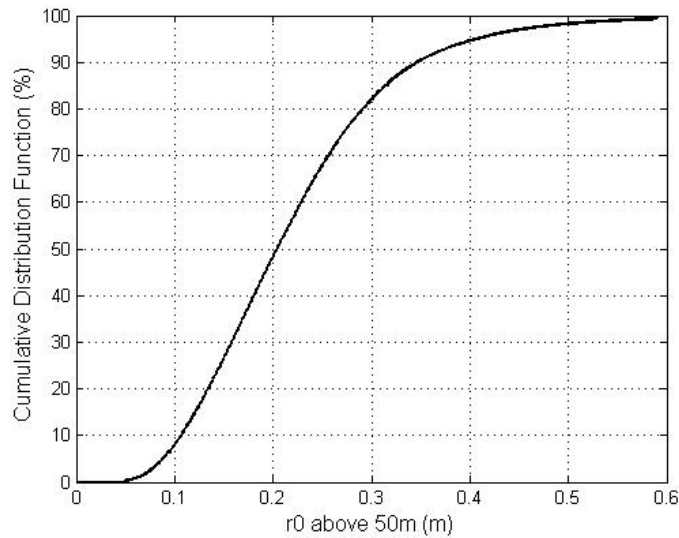


Figure 2. Cumulative distribution function of r_0 above 50m

3.3 Telescope orientation

A record of telescope azimuth and elevation angles has been obtained from Gemini North for the year 2005. It was then mapped to 2006 and repeated for 2007. The telescope zenith angle (azimuth averaged) probability distributions are shown in Figure 3. Even though this probability distribution can in general be similar to that expected for TMT, the actual record will not correspond to real targets viewed from Armazones. Alternatively, similar records can be produced for any given latitude, tailored to TMT.

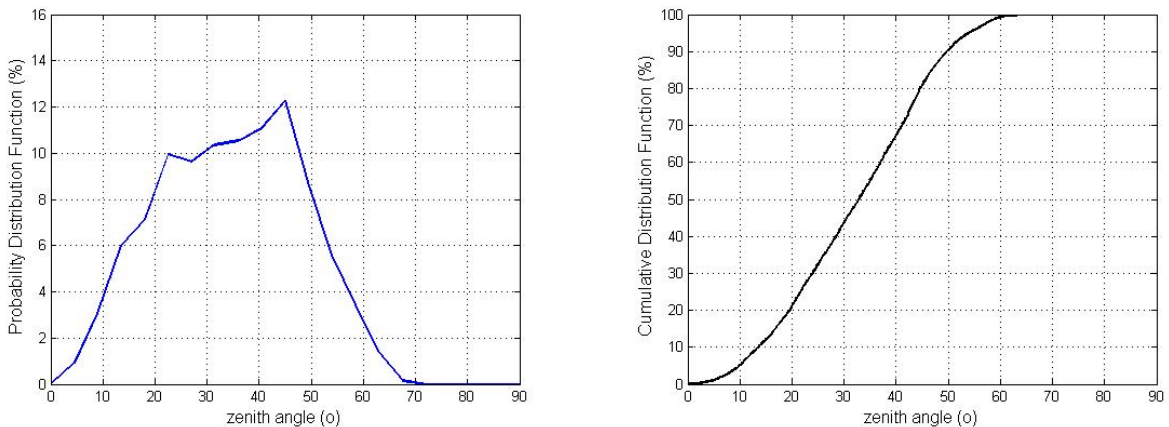


Figure 3. Probability distribution (left) and cumulative distribution function (right) for telescope zenith angle

4. MODELING

4.1 Models incorporated

Modeling and Analysis for Controlled Optical Systems tool (MACOS) developed by JPL [3]. The output is a function of the telescope zenith angle and the M1 temperature relative to the M1 temperature during the last APS measurement.

TMT integrated dynamic disturbance model (DOCS) [4]. The output is a function of the telescope zenith angle, the relative to wind azimuth angle and the external wind speed.

TMT dome seeing model [5]. The output is a function of the telescope zenith angle, the relative to wind azimuth angle and, implicitly, the external wind speed.

Since the PSSn seeing limited metric depends on the atmospheric seeing, all aberration matrix elements are in fact PSSn values and the matrices have an additional dimension which is the atmospheric r_0 .

Additional models provide input to the framework or the above models. They include CFD simulations of the Segment Support Assembly and the Observatory on the candidate summit [6], the radiation-convection lumped-mass model [6], and the solid thermal model of the Segment Support Assembly [7].

The only model that has to run simultaneously with the Framework is the TMT mirror seeing model [5]. It accepts a map of temperature differences between M1 surface and the ambient air temperature 10cm above M1 and yields a PSSn value based on the current r_0 . The M1 thermal model that tracks the M1 surface temperature is briefly presented in the next section.

4.1.1 M1 thermal model

The purpose of this model is to calculate the temperature difference between M1 front and the ambient air that is required to estimate mirror seeing. The deviation of M1 temperature with respect to its temperature during the last APS measurement is also provided. Since the temperature field of a solid object has a long time-scale (“memory”) the calculation has to be unsteady and run fast as part of the Framework. The model should be able to resolve the spatial distribution of the heat source behind M1 and of the heat transfer coefficient variations on M1 front for different telescope orientations.

The one-dimensional transient heat conduction equation is solved for M1 temperature T , using fluxes for boundary conditions:

$$\frac{\partial T}{\partial t} = \frac{k}{\rho c_p} \frac{\partial^2 T}{\partial z^2}, \quad -k \frac{\partial T}{\partial z} = q_{\text{boundaries}}$$

For the front surface a radiation out-flux of 0.4W/m^2 and a convective out-flux of $h(T-T_A)$ are used. Gaussian fluctuations are superimposed on air temperature T_A to capture the effect of M1 surface micro-turbulence. The heat transfer coefficient maps are obtained from CFD. For the back surface a variable net heat in-flux is used ($0.5\text{-}2.5\text{W/m}^2$), generated by FEA and CFD modeling.

The back surface uses 19 points per segment in the horizontal direction based on the distribution of the heat sources on the SSA (actuators and edge sensor preamplifiers). Both back and front fluxes are then interpolated on a 120×120 grid with a 0.25m resolution. In the normal direction the segment can be split into a maximum of 4 layers.

4.1.2 Parameter ranges

Zenith angle: $0^\circ - 65^\circ$

Azimuth angle relative to wind: $0^\circ - 180^\circ$

External wind speed: $0\text{-}16\text{m/s}$

Difference between current M1 temperature and M1 temperature at last APS calibration: $0\text{-}10\text{K}$

Atmospheric r_0 : $0.05\text{-}0.6\text{m}$

4.2 Assumptions – operating conditions

The enclosure aperture opens at sunset and closes at sunrise.

The telescope orientation record has the information on non-observing time incorporated. Therefore, while the mirror temperature is being tracked, only the performance values under observing time are statistically processed. When the external wind speed is above 16m/s the mode is considered non-observing. The first hour after sunset is also excluded from the statistics.

In order to consider a night record fit for simulation significant portions of continuous temperature values should exist past sunset. The record is filtered and, whenever possible, gaps of missing or corrupted data are interpolated. Nights with less than three hours of data are discarded.

If the models use the weather record of Mauna Kea, then the Gemini North telescope record will be correlated with the weather record. Non-observing time due to weather will be correctly accounted for, but the telescope orientation in observing mode will be a result of the Gemini queue-observing model as well as venting and wind buffeting mitigation strategies (wind direction correlation). By using the Armazones data, however, no correlations whatsoever can exist, thus rendering the process a true Monte Carlo simulation. That will result in a conservative estimate of the TMT performance.

As mentioned above the external wind speed and temperature at 20m have been scaled from 2m. The same scale factors are applied to all wind directions.

The external wind speed scaled from 2m to 20m above the undeveloped site is similar to the expected wind speed two dome diameter upwind of the developed site (see appendix).

It is assumed that the primary mirror will be pretreated during the day by air-conditioning. The starting temperature can be from the previous night (at n hours after sunset) or can be a fixed difference from the sunset temperature (currently at -2K).

APS measurements are taken every 15 days (currently at three hours after sunset). The start of the 15-day cycles was arbitrary (first night with available temperature data).

The wind speed above M1 is assumed to be controlled at 1m/s by modifying the vent area. Velocity on M1 varies linearly as a function of open vent area [6].

Since the TMT enclosure is a Calotte design, venting efficiency is not considered symmetric with respect to the axis normal to elevation. The efficiency factor is defined as the ratio of delivered wind speed above m1 to the external wind speed. It is assumed, however that the well vented side faces upwind when two enclosure orientation solutions are possible for the same relative to wind azimuth angle.

4.3 Errors modeled

The modeled errors can be grouped in three major categories. Surface shape errors, alignment errors and thermal seeing. The aberrations estimated for TMT consist of individual errors, the product of whose equals the total. Since the PSSn metric is multiplicative between errors that are considered independent (assumption valid for short time-scales) [8] the product of the estimated individual expectations (means) $\prod \langle E_i \rangle$ should be equal to the total expectation $\langle E_T \rangle$ as long as the errors are also independent during the period examined by the Framework. It will be shown that this is also a valid assumption. Thus an overall performance allocation based on an ensemble average of operating conditions rather than representative operating points can be defined and decomposed (top-down error budget). The estimated mean of an error $\langle E_i \rangle$ can be compared to its corresponding allocation and the total expectation can be compared to the overall allocation (bottom-up verification).

In this study we will focus on certain representative error estimates. More specifically, the segment figuring residual, which is the single largest error contributor, will be studied separately. From the remaining M1 segment shape errors, support print-through, thermal distortion, in-plane displacement, out-of-plane residual and segment dynamic displacement residual, the fabrication print-through, the installation and gravity and sensor and actuator noise are not modeled. M2 shape errors and M3 shape errors (figuring and print-through) that do not include fabrication print-through, thermal distortion and dynamic shape residual errors will also be presented. The APS alignment error will be incorporated in the shape error. From the dynamic alignment errors only wind seeing is studied. And thermal seeing consists of mirror and dome seeing.

5. RESULTS

5.1 Expected Image Quality

Figure 4 presents the cumulative distribution function of the estimated TMT errors in PSSn metric values. The expectation (mean) of the distribution is noted. The conditional distribution of mean values, which retains performance information under various seeing conditions, is shown in Figure 5.

Table 1 summarizes the expectations for the different modeled errors. The validity of the normalized PPS metric's ability to produce individual independent errors can be easily verified. For instance, the total optical error mean is 0.87290, while multiplying the two M1, M2 and M3 error means yields 0.87265, a 0.05% deviation.

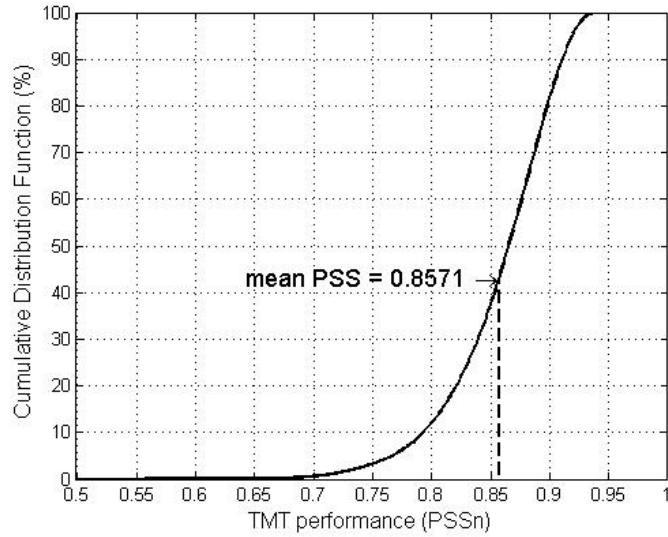


Figure 4. Cumulative Distribution Function of total TMT performance in PSSn

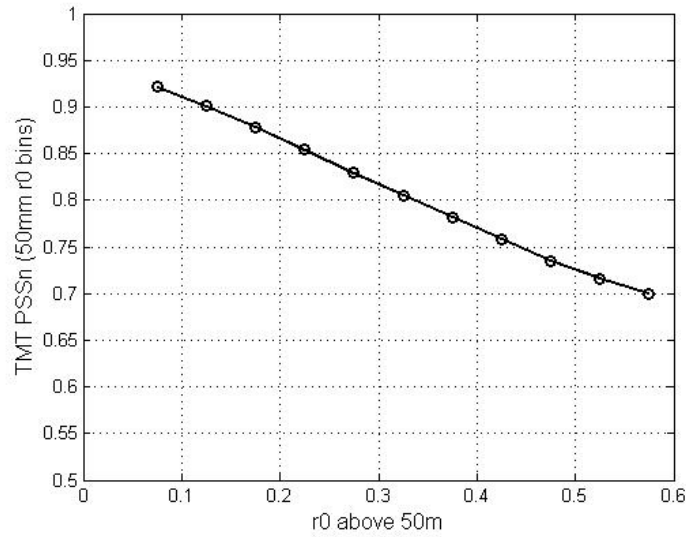


Figure 5 Conditional mean distribution varying with atmospheric r_0 (right) of total TMT performance in PSSn

Table 1. Modeled error estimates

Description	Estimate (expectation)		
	Segment figuring residual	0.95154	0.91195
Remaining M1 terms	0.95808		
M2 shape		0.97473	
M3 shape		0.98171	
Wind seeing			0.99807
Mirror seeing		0.99558	0.98310
Dome seeing		0.98744	
TMT			0.85710

5.2 Sensitivity analysis

There are certain parameters that are readily adjustable in the Framework so that their effect on performance and the corresponding sensitivity can be assessed. The heat sources behind M1 can be adjusted, even though the current values are a result of detailed thermal analysis. The type of daytime mirror treatment as already explained can be investigated. Table 2 shows the median value of the spatially averaged temperature difference between M1 and the air above it for three different initial mirror temperatures. First, the temperature of the previous night three hours after sunset is used. Alternatively a fixed offset from the ambient sunset temperature is used, at -2.5K (mirror is cooler). It appears that the second method show a considerable decrease in the temperature difference. This is expected since it eliminates weather variability effects on a 24h scale, but is requires prediction of sunset temperature. Apparently, see third case, the required accuracy of the prediction is not high. The current treatment has already incorporated the results of that exercise. The same hold true for the APS measurement frequency. Table 3 presents the median and 90%ile values of the M1 temperature difference between APS measurements for four different intervals. It appears that a good compromise between thermal distortion effects and time lost due to measurements is 15 days. Another important parameter is the proper r_0 value to represent the atmosphere above 60m. Based on combined DIMM, MASS, and SODAR measurements and depending on the strength of the ground layer, the expected r_0 should be a combination of the DIMM and MASS values with weight factors anywhere from 0.3 to 0.7. If, instead of 0.5 for both, we select 0.6 for DIMM and 0.4 for MASS the overall PSSn expectation shifts only by 0.6% (0.863 instead of 0.857). Therefore the choice of appropriate reference r_0 value will not affect the essence of the performance results.

Table 2. Mirror temperature treatment sensitivity study

Starting M1 temperature	Median $ T_M - T_A $ (K)
3h after sunset of previous night	0.64
2.5K below sunset	0.56
1.0K below sunset	0.55

Table 3. APS measurement frequency sensitivity study

APS measurement frequency (days)	$ T_M - T_{M_{APS}} $ (K) median (left)-90% (right)	
5	1.30	4.01
10	1.86	4.86
15	1.84	4.73
30	1.92	5.35

Finally, the venting efficiency and the wind reduction factors for telescope wind buffeting can also be free parameters, even though they are results of the enclosure design. However, it can be shown how sensitive TMT performance can be to those parameters before a design modification effort takes place.

6. CONCLUSIONS

The simulation framework makes use of the PSSn metric multiplicative property to enable top-down and bottom-up error budgeting for the range of expected operating conditions rather than characteristic operating points.

It offers probability distributions of errors to denote the range of expected performance under various seeing conditions, knowledge particular useful to queue observing.

It allows us to investigate the behavior of the observatory on different candidate sites. In fact a similar effort to the one described above is currently underway for Mauna Kea, Hawaii.

It can be used to optimize certain operating strategies, such as venting, daytime mirror thermal treatment and APS measurement frequency.

Finally, it can unveil the true impact of a particular design decision to the expected observatory performance and subsequent science productivity, enabling cost-effective trade-offs.

We have developed a time domain Monte Carlo Framework for performance estimates and requirement validation for TMT. Its output enables us to estimate the magnitude of the optical effect of various disturbances and aberrations on the telescope performance, their relative importance and sensitivity to a wide range of environmental and operational

parameters. Thus it is a useful tool for adjusting performance goals, balancing the system error budget and setting design specifications.

ACKNOWLEDGMENTS

The authors would like to thank Matthias Schöck (TMT site selection manager) who provided the records of environmental parameters. They also acknowledge the contribution of Douglas MacMynowski (Caltech), Carl Nissly (JPL) and John Pazder (HIA) who provided the framework with look-up tables of performance estimates, as well as the Gemini North Observatory for the record of telescope orientations.

The authors gratefully acknowledge the support of the TMT partner institutions. They are the Association of Canadian Universities for Research in Astronomy (ACURA), the California Institute of Technology and the University of California. This work was supported as well by the Gordon and Betty Moore Foundation, the Canada Foundation for Innovation, the Ontario Ministry of Research and Innovation, the National Research Council of Canada, and the U.S. National Science Foundation.

APPENDIX

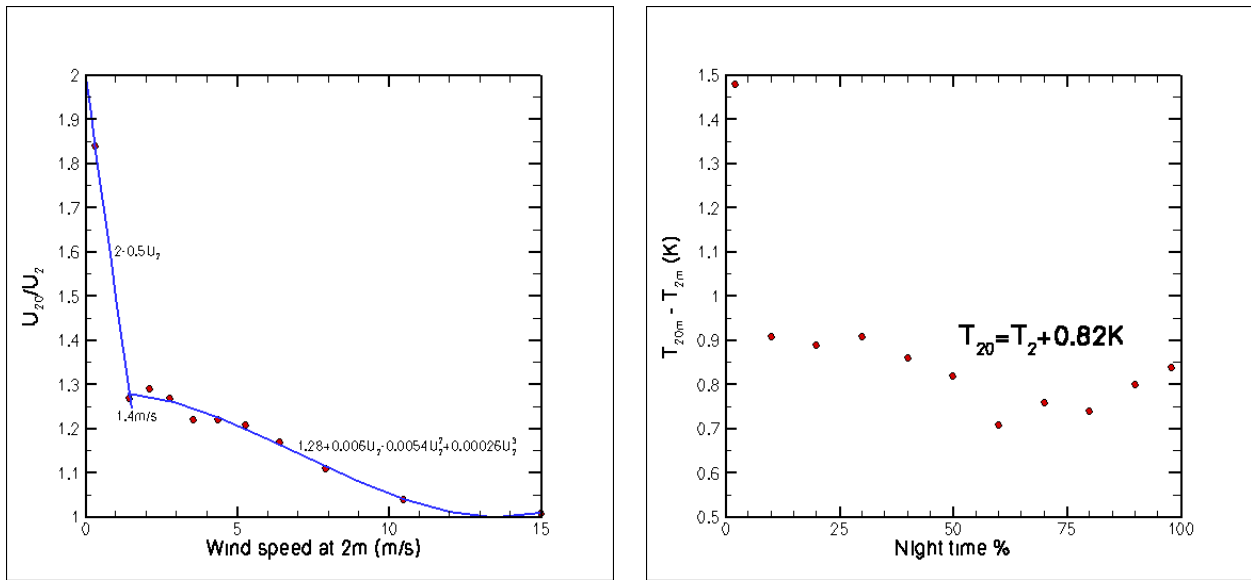


Figure A1. (a) Wind speed factor between 2m and 20m (left) and (b) the corresponding temperature factor (right)

Out of the 729 nights there exist only 353 nights with simultaneous weather, telescope and atmospheric r0 data. The number of available time-steps for statistics (“observing mode”) is 23.5% of the total. Even though there is no loss of seasonal variability, we investigated the impact of data loss to the environmental statistics, especially wind speed. The resulting median wind speed for the period is 7.6m/s, which drops to 7.2m/s if the 16m/s operating restriction is imposed. When only the time-steps that contain r0 values are considered the resulting median is closer to 6.2m/s. Given the operating limitations of the DIMM and MASS instruments at high winds, one would assume that the data record is biased. In reality the two instruments experienced some downtime in 2007 (which was a windy year), that was unrelated to environmental conditions. Moreover, simulations showed that the actual reference wind speed for the Framework will be at least 10% lower than the value measured from the Armazones tower at 20m. Figure A2 depicts why.

For a reference wind speed boundary condition of 7m/s the wind accelerates to 7.8-8m/s at the 20m-30m level above the undisturbed site (solid curve). But the wind reduction factors, venting efficiencies and resulting heat transfer coefficients are estimated based on the upwind wind speeds. At two dome diameters upwind of the observatory the flow is already experiencing deceleration (~6.8m/s, dashed curve). So there is a reduction factor of about 7/8 in expected median wind

conditions, which will bring the aforementioned 7.2m/s value down to 6.3m/s. Therefore the loss of above average wind 2007 r0 data should not affect the expected statistical behavior of wind buffeting.

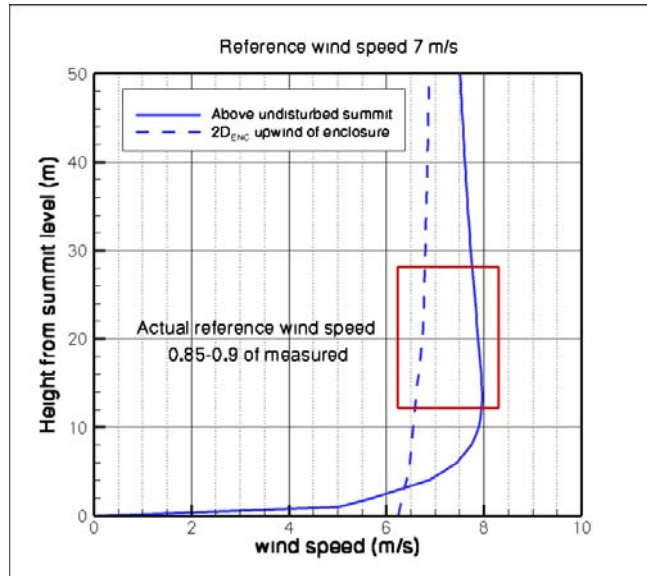


Figure A2. Vertical wind profiles above Armazones calculated by CFD

REFERENCES

1. Angeli, G. Z., Roberts, S., Vogiatzis, K., "Systems engineering for the preliminary design of the Thirty Meter Telescope", SPIE 7017-3, Marseilles France, 2008.
2. Schöck, M. et al, "Status of the Thirty Meter Telescope site selection program", SPIE 7012-68, Marseilles France, 2008.
3. Nissly, C. R. et al, "High-resolution optical modeling of the Thirty Meter Telescope for systematic performance trades", SPIE 7017-30, Marseilles France, 2008.
4. MacMynowski, D. G., Blaurock, C., Angeli, G. Z., "Dynamic analysis of TMT", SPIE 7017-31, Marseilles France, 2008.
5. Pazder, J., Vogiatzis, K., "Dome and mirror seeing estimates for the Thirty Meter Telescope", SPIE 7017-26, Marseilles France, 2008.
6. Vogiatzis, K., "Advances in aero-thermal modeling for TMT", SPIE 7017-25, Marseilles France, 2008.
7. Cho, M., Corredor, A., Pootrakul, S., Vogiatzis, K., "Thermal performance prediction of the TMT optics", SPIE 7017-43, Marseilles France, 2008.
8. Seo B.-J. et al, "Analysis of Point Source Sensitivity as a performance metric for the Thirty Meter Telescope", SPIE 7017-28, Marseilles France, 2008.